Environmental Science
Processes & Impacts

PAPER

View Article Online
View Journal | View Issue

Cite this: *Environ. Sci.: Processes Impacts*, 2015, **17**, 1587

A first look at the influence of anthropogenic climate change on the future delivery of fluvial sediment to the Ganges–Brahmaputra–Meghna delta

Stephen E. Darby,*[a] Frances E. Dunn,[a] Robert J. Nicholls,[b] Munsur Rahman[c] and Liam Riddy[a]

We employ a climate-driven hydrological water balance and sediment transport model (HydroTrend) to simulate future climate-driven sediment loads flowing into the Ganges–Brahmaputra–Meghna (GBM) mega-delta. The model was parameterised using high-quality topographic data and forced with daily temperature and precipitation data obtained from downscaled Regional Climate Model (RCM) simulations for the period 1971–2100. Three perturbed RCM model runs were selected to quantify the potential range of future climate conditions associated with the SRES A1B scenario. Fluvial sediment delivery rates to the GBM delta associated with these climate data sets are projected to increase under the influence of anthropogenic climate change, albeit with the magnitude of the increase varying across the two catchments. Of the two study basins, the Brahmaputra's fluvial sediment load is predicted to be more sensitive to future climate change. Specifically, by the middle part of the 21st century, our model results suggest that sediment loads increase (relative to the 1981–2000 baseline period) over a range of between 16% and 18% (depending on climate model run) for the Ganges, but by between 25% and 28% for the Brahmaputra. The simulated increase in sediment flux emanating from the two catchments further increases towards the end of the 21st century, reaching between 34% and 37% for the Ganges and between 52% and 60% for the Brahmaputra by the 2090s. The variability in these changes across the three climate change simulations is small compared to the changes, suggesting they represent a significant increase. The new data obtained in this study offer the first estimate of whether and how anthropogenic climate change may affect the delivery of fluvial sediment to the GBM delta, informing assessments of the future sustainability and resilience of one of the world's most vulnerable mega-deltas. Specifically, such significant increases in future sediment loads could increase the resilience of the delta to sea-level rise by giving greater potential for vertical accretion. However, these increased sediment fluxes may not be realised due to uncertainties in the monsoon related response to climate change or other human-induced changes in the catchment: this is a subject for further research.

Received 2nd June 2015
Accepted 31st July 2015

DOI: 10.1039/c5em00252d

rsc.li/process-impacts

Environmental impact

To develop better estimates of the sustainability of coastal environments, including the world's vulnerable deltas, requires estimates of the rate at which fluvial sediment is supplied to the coastal zone. Unfortunately, the current state of the science is that such estimates are lacking. This study presents the first attempt to model the plausible impacts of anthropogenic climate change on the delivery of fluvial sediment to the Ganges–Brahmaputra–Meghna (GBM) delta, one of the world's largest and most populous river delta systems. We show that climate change may significantly increase the future delivery of fluvial sediment to the GBM delta, data that will help underpin assessments of the future sustainability and resilience of one of the world's most vulnerable mega-deltas.

1. Introduction

The quantification of the flux of terrestrial sediment from catchments to the oceans is an important scientific challenge.[1] Sediment flux dynamics play a key role in the Earth's geology[2] and biogeochemistry,[3,4] while significantly influencing the lives of the 500 million people who inhabit the world's river deltas.

[a]*Geography and Environment, University of Southampton, Highfield, Southampton SO17 1BJ, UK. E-mail: S.E.Darby@soton.ac.uk*
[b]*Engineering and the Environment and Tyndall Centre for Climate Change Research, University of Southampton, Highfield, Southampton, SO17 1BJ, UK*
[c]*Institute of Water and Flood Management, Bangladesh University of Engineering and Technology, Dhaka-1000, Bangladesh*

This is because deltas are depositional land features whose very existence is dependent on the continued supply of fluvial sediment that created them.

Yet the inhabitants of the world's deltas are becoming increasingly vulnerable to flooding, and conversions of their land to open ocean due to rising relative sea levels.[5,6] The degree to which delta surfaces are undergoing vertical changes relative to local mean sea level (ΔRSL) can be understood to be the result of a complex interplay between five main factors:

$$\Delta\mathrm{RSL} = A - \Delta E - C_\mathrm{N} - C_\mathrm{A} \pm M \quad (1)$$

such that if a delta is not to be 'drowned' by rising sea-levels, the delta surface aggradation rate (A) must equal or exceed the sum of the eustatic sea-level rate (ΔE) and subsidence associated with the natural (C_N) and/or accelerated (C_A) rate of compaction of the deltaic deposits, the latter being an anthropogenic component related to activities such as water and gas extractions, and other vertical movements of the land surface (M) associated, for example, with tectonics.[6]

Based on an overview of the trajectories of these five parameters in 33 representative deltas, Syvitski *et al.*[6] conservatively estimated that the area of deltas that are vulnerable to flooding could increase by as much as 50% during the twenty-first century under current projected values for sea-level rise. For many of the world's deltas, even if it is frequently difficult to separate the precise contribution of the terms C_N, C_A and M, the dominant contribution to rising relative sea-level is often land subsidence. For example, subsidence rates ranging from 50 to 200 mm per year have been observed in the Chao Phraya delta,[7] while in the Ganges–Brahmaputra delta recent satellite based estimates indicate that subsidence rates vary in the range 0 to 18 mm per year.[8,9] Meanwhile, global mean sea-level is currently (1993–2010) rising at 3.2 $\pm$ 0.4 mm per year,[10] increasing to as much as 8 to 16 mm per year by the end of the century.[11] Consequently, variations in delta surface aggradation rates (typically of the order of a few mm per year, but in some cases reaching 50 mm per year) can potentially balance the negative effects of subsidence and eustatic sea-level rise. Since delta surface aggradation is dominantly controlled by the rate of supply of fluvial sediment, this supply of fluvial sediment can be viewed as a key factor in sustaining delta surfaces above mean sea level, or at least delaying the onset of drowning. Indeed, anthropogenic disturbance, notably through soil conservation and damming, is invoked as a key historical driver for a significant (>30%) global reduction in fluvial sediment flux during the latter half of the twentieth century,[12–16] further adding to the contemporary pressures on vulnerable deltas.[6] This relatively recent reduction in sediment flux sits within the longer historical context that sediment fluxes previously tended, in many river systems, to be artificially high due to deforestation and other poor land-use practices.[6] Meanwhile, in some cases, most notably the Mississippi River Delta, researchers have advocated that restoration of (disconnected) fluvial sediment supplies is a potential means to naturally engineer delta building.[17,18]

Therefore, to develop better estimates of the sustainability of fragile coastal environments, including the world's vulnerable deltas, there is a clear need to have accurate estimates of the fluvial sediment flux. Unfortunately, the current state of the science is that such estimates are lacking. Many authors have commented on the general lack of reliable empirical data of sediment flux to the earth's coastal systems, but investigations of the responses of sediment flux to *future* environmental change requires the application of sophisticated numerical models. Despite advances made in recent years[1,2,19,20] this form of modelling remains challenging and very few *predictive* studies of fluvial sediment delivery under projected environmental changes have yet been undertaken. A notable exception is the recent study by Cohen *et al.*,[1] albeit this investigation was focused on *historical* (1960–2010) trends at the global scale, such that there remains a clear need for prognostic regional studies.

To address this significant research gap, in this study we present the first effort to model the plausible impacts of anthropogenic climate change in the 21st century on the delivery of fluvial sediment to the Ganges–Brahmaputra–Meghna (GBM) delta. We focus on the GBM delta because the combined water ($\sim$1.07 km^3 per year) and sediment (>1 Gt per year[21]) discharges from the Ganges and Brahmaputra catchments (note that we exclude the Meghna from consideration in this study as its sediment flux of around 13 Mt per year[22] is negligible in relation to the contributions from the Ganges and Brahmaputra) have built one of the world's largest ($\sim$115 000 km^2 (ref. 23)) and most populous (>110 million[23]) river delta systems. Moreover, the massive sediment loads delivered from the GBM catchments are, at least under pristine conditions, sufficient to drive aggradation ($\sim$3.5 mm per year) that is sufficient to compensate for slow sea-level rise and subsidence.[8,9,21,24,25] For all these reasons, the GBM presents an ideal system to investigate whether climate-driven changes in future fluvial sediment flux could compensate for (or compound) the adverse impacts of accelerated global sea-level rise and anthropogenic subsidence, particularly as the lives and livelihoods of so many people are at stake. To this end, we employ a well-established model (HydroTrend;[19] see below), parameterised and validated for the GBM catchments, and forced by daily temperature and precipitation data obtained from downscaled Hadley Centre (HadRM3P) Regional Climate Model (RCM) runs for the period 1971–2100. Specifically, three realizations (here termed Q0, Q8 and Q16; see Section 2.3 for details) representing different sets of perturbed climate model runs are used to help quantify uncertainties in the range of future climate conditions simulated by HadRM3P under the SRES A1B scenario. The new data obtained in this study offer the first estimate of whether and how anthropogenic climate change may affect the delivery of fluvial sediment to the GBM delta, informing assessments of the future sustainability and resilience of one of the world's most vulnerable mega-deltas.

2. Methods

2.1. Model selection and description

In this study we selected HydroTrend v.3.0 (ref. 19) (henceforth we refer to the model simply as HydroTrend), a climate-driven hydrological water balance and transport model, to simulate

water discharge and sediment load at defined outlets of the two study catchments (see below and Fig. 1 for details of catchment outlet locations). HydroTrend is a lumped catchment model and consequently is both relatively simple to parameterise and fast to run. It may be considered to be a first order model that describes the major processes controlling fluvial sediment supply from drainage basins, making it suitable for estimating water fluxes and sediment loads over time scales that range from 10^1 to 10^5 years.[19] Its use here may be justified by the model's successful application in prior studies which have considered (i) the effects of climate change and glacier fluctuations on sediment fluxes from the Po River basin over the last 21k years;[26] (ii) long term sediment fluxes to the coastal zone emanating from the Waipaoa River in New Zealand;[27,28] and, (ii) the effects of reservoirs on fluvial sediment flux.[29] Full details of the model development and implementation are provided by Kettner and Syvitski,[19] but a short summary is now provided for the sake of completeness.

HydroTrend first generates daily water discharges (Q) at the defined river mouth by computing the balance between precipitation per unit area (P) and evaporation (E), but modified by water storage and release (Sr), such that:

$$Q = P - E \pm \mathrm{Sr} \quad (2)$$

The water balance expressed by eqn (2) is computed through the simultaneous partitioning of five runoff processes at the daily time scale, namely rain (Q_r), snowmelt (Q_n), glacial melt (Q_{ice}), groundwater discharge (Q_g) and evaporation (Q_{Ev}) such that:

$$Q = Q_r + Q_n + Q_{ice} - Q_{Ev} \pm Q_g \quad (3)$$

The various terms in eqn (3) are computed following Syvitski and Alcott[30] and Syvitski *et al.*[31] In brief, the basin climate (temperature and precipitation), together with a user-defined lapse rate (see Section 2.2), is used to determine the freezing line altitude (FLA) and thus the partitioning of precipitation into rain or snowfall.[19] Together with information about the basin topography (see Section 2.2), the time-varying FLA is then used to determine the basin areas required for the snow and rain subcomponents in eqn (3). By similar means the glacier equilibrium line altitude (ELA) is employed to determine the proportion of the simulated basin covered by glaciers. HydroTrend also accounts for the influence of basin geometry and river length in delaying the contribution of each of the

Fig. 1 Map of the Ganges and Brahmaputra catchments in south Asia showing the catchment topography and the locations of the basin outlets (marked F for Farakka Barrage on the Ganges and J for the confluence of the Jamuna and Ganges for the Brahmaputra) used to simulate sediment fluxes. The locations of gauging stations referred to in the text are also indicated.

hydrological subcomponents to the water discharge at the basin outlet and likewise estimates the influence of discharge attenuation by lakes and reservoirs (see Syvitski and Alcott[30]).

Having computed the discharge at the basin outlet, HydroTrend next estimates the sediment discharge (Q_s) using a suite of semi-empirical relationships to account for both suspended sediment load and bedload, with an empirical function being employed to account for differences in sediment production related to fluctuations in glacier extent. Sediment load is then predicted using the *BQART* module[4] where:

$$Q_s = \omega \times B \times Q^{0.31} \times A^{0.5} \times R \times T \text{ (for } T \geq 2\ ^\circ\text{C)} \quad (4a)$$

and

$$Q_s = 2 \times \omega \times B \times Q^{0.31} \times A^{0.5} \times R \text{ (for } T < 2\ ^\circ\text{C)} \quad (4b)$$

with A and R the drainage basin area and maximum relief, T the basin-averaged temperature, ω a coefficient of proportionality defined as $\omega = 0.02$ kg s^{-1} km^{-2} °C^{-1}, and B is a factor to account for the influence of lithology, sediment trapping efficiency of reservoirs and anthropogenic disturbance of land cover on the supply of sediment to the fluvial network. The factor B is given by:

$$B = L(1 - T_e)E_h \quad (5)$$

where L is the lithology factor and E_h an anthropogenic disturbance factor (see Section 2.2 for details of these two parameters). Finally, the sediment trapping efficiency of reservoirs (T_e) is computed using the methods of Brown[32] for small (<0.5 km^3) reservoirs or Brune[33] and Vörösmarty *et al.*[34] for larger (≥0.5 km^3) water bodies (see Kettner and Syvitski[19] for details). As implemented in this study, both the water and sediment discharges are simulated at a daily temporal resolution.

2.2. Model parameterisation

HydroTrend models for the Ganges and Brahmaputra catchments investigated in this study were set up by initially defining the locations of the respective catchment outlets (Fig. 1): (1) at the Farakka Barrage (at 24.80°N 87.93°E) in eastern India for the Ganges, and; (2) at the confluence of the Jamuna River with the Ganges in Bangladesh (at 23.82°N 89.75°E; note that the Brahmaputra in Bangladesh is referred to as the Jamuna River). These specific locations were selected as they may be considered to be key boundary nodes for simulating the influx of sediment from the dominant fluvial arteries into the GBM mega-delta complex. Locations further downstream were not selected to avoid the need to simulate delta distributary channels, whereas locations upstream are less representative of the sediment influx conditions to the delta. The topography of the drainage basins upstream of these catchment outlets was represented using hypsometric curves (Fig. 2), which express the drainage area contained within each of a series of elevation bins (spaced in this study at 25 m vertical intervals). The topographic data used to compute these hypsometric curves were modelled using the Advanced Spaceborne Thermal Emission and Reflection Radiometer (ASTER) Global Digital Elevation Model (GDEM) product,[35] with the drainage area in each elevation bin extracted using standard measurement tools within ArcGIS. The ASTER GDEM is a product of the Japanese Ministry of Economy, Trade, and Industry (METI) of Japan and the United States National Aeronautics and Space Administration (NASA) and comprises a 1 arc-second (~30 m) resolution grid of elevation postings referenced to the WGS84/EGM96 geoid, with an estimated accuracy (at 95% confidence) of 20 m and 30 m in the vertical and horizontal planes, respectively.

The remaining parameter values used to characterise the biophysical properties of the two study catchments may be categorised into parameters whose values may be defined by direct measurement (the 'physical parameters' listed in Table 1) and those whose values are not directly measurable ('calibration parameters' in Table 1). Of the physical parameters, the length of the rivers (RivL) and floodplain gradients (S) upstream of the basin outlets were both extracted from the catchment DEMs described above, again using standard measurement tools within ArcGIS. We assumed that the lapse rate, LR, and initial equilibrium line altitude, ELA_0 (used in HydroTrend, together with a forcing temperature time series (see below) and basin hypsometry, to determine the proportion of the modelled catchments covered in glacial ice), were both identical for the two catchments, with their values being selected with reference to the International Civil Aviation Organization standard and Ya-feng *et al.*,[36] respectively (Table 1). The baseflows (Q_{base}) for the respective catchments equated to the mean annual flow minima as estimated from hydrological records for the gauging stations located at Hardinge (period of record 1973–1995) on the Ganges and Bahadurabad (1973–1995) on the Brahmaputra (see Fig. 1 for gauge locations). The storage capacities of reservoirs (R_{Vol}) were determined from Lehner *et al.*,[37,38] noting that the only significant large reservoir in the baseline period (*cf.* Fig. 1) is the Farakka Barrage on the Ganges. The lithology factor (L) is a factor in the BQART model to account for surface resistance to erosion, and was parameterised following Syvitski and Milliman.[4] Similarly, E_h is another factor in the *BQART* model and accounts for the effects of anthropogenic disturbance on suspended sediment flux, with the value of E_h being

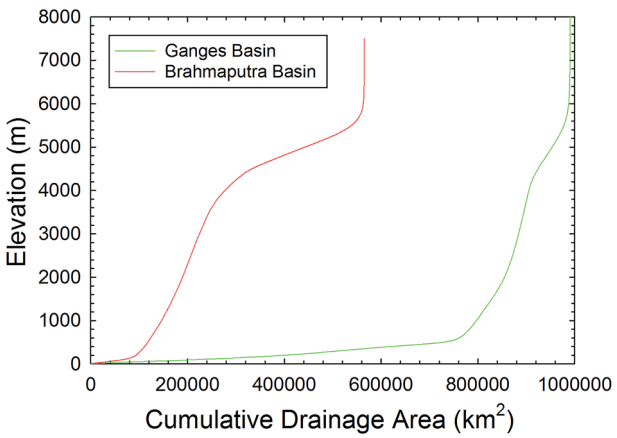

Fig. 2 Hypsometric curves for the Ganges and Brahmaputra basins.

parameterised based on population density and GNP per capita.[4,19]

For the calibration parameters listed in Table 1, sensitivity analyses revealed that variations in the dry precipitation evaporation fraction (DPEF), saturated hydraulic conductivity (K_0), subsurface flow coefficient (f), and the subsurface flow exponent (g) all had a negligible effect on model behaviour. Therefore the values of these parameters were set to the middle of the ranges recommended by Kettner and Syvitski.[19] The hydraulic geometry parameters (k, m, a, b) were estimated using values taken from Clifford,[39] with the average river velocity parameter (V_{mean}) then being derived from these hydraulic geometry parameters for internal consistency. The maximum groundwater parameter (GWV_{max}) was found to have a significant effect on peak water discharge and so was used as a calibration parameter by fitting simulated (for the Q0 model runs) to measured water discharges. The initial groundwater value (GWV_0) was set at the value output by HydroTrend after running the models for a 1000 year 'spin-up' using the first year of climate data repeated (for both the Ganges and Brahmaputra catchments) to ensure that there were no trends in the groundwater value at the start of the model runs which might influence water discharge output. The minimum groundwater parameter (GWV_{min}) was set to the minimum possible to allow the full potential range of groundwater values to be expressed.

The complete set of parameter values employed in the simulations reported herein is listed in Table 1. Using these parameters, HydroTrend was employed to simulate water and sediment fluxes at the study catchment outlets, for the climate change scenario discussed in the next section. The model was in all cases run continuously at a daily resolution for the period 1971–2100.

2.3. Anthropogenic climate change

The climate data used in this study were derived from an existing set[40] of regional climate model (RCM) simulations

Table 1 List of HydroTrend parameter values employed in this study. The table groups model parameters into those that are determined *via* physical measurement/consideration, and those whose values are not known *a priori* and which must therefore be determined by calibration and/or expert judgement (see text for details)

			Values used for study catchments in baseline (1981–2000) simulation period	
Symbol	Units	Description and notes	Ganges	Brahmaputra
Physical parameters				
Q_{base}	$m^3\ s^{-1}$	Mean annual base flow in the catchment	880	4020
LR	C km^{-1}	Lapse rate used to calculate temperature in altitude bins	6.4	6.4
ELA_0	m	Initial glacier equilibrium line altitude	5500	5500
S	m m^{-1}	Floodplain gradient at model outlet. Determined from basin DEM	8.27×10^{-5}	1.83×10^{-4}
RivL	km	Length of main river channel upstream of outlet	2525	2900
R_{Vol}	km^3	Reservoir storage capacity	42.0	6.8
L	—	Factor to reflect the influence of the catchment substrate on resistance to erosion[4]	1.05	1.10
E_h	—	Factor to reflect the influence of anthropogenic disturbance on sediment production. Determined as a function of population density and GNP per capita[4]	2.0	2.0
Calibration parameters				
DPEF	—	Dry precipitation evaporation fraction (*i.e.* the fraction of dry precipitation (nival and ice) which will be evaporated)	0.45	0.45
K_0	mm per day	Saturated hydraulic conductivity	85.0	85.0
k	m^{-2}	Coefficient in hydraulic geometry equation $V = kQ^m$ used to compute velocity (V) at the basin outlet (Q = flow discharge)	0.084	0.084
m	—	Exponent in hydraulic geometry equation $V = kQ^m$ used to compute velocity (V) at the basin outlet (Q = flow discharge)	0.34	0.34
a	s m^{-2}	Coefficient in hydraulic geometry equation $W = aQ^b$ used to compute width (W) at the basin outlet (Q = flow discharge)	197.4	197.4
b	—	Exponent in hydraulic geometry equation $W = aQ^b$ used to compute width (W) at the basin outlet (Q = flow discharge)	0.26	0.26
V_{mean}	m s^{-1}	Average river velocity, used in flow routing computations	2.0	2.0
GWV_{max}	m^3	Maximum groundwater pool storage	4.3×10^9	6.0×10^8
GWV_{min}	m^3	Minimum groundwater pool storage	1.0	1.0
GWV_0	m^3	Initial groundwater pool storage	5.76×10^8	6.0×10^8
f	$m^3\ s^{-1}$	User defined coefficient used to control the draining of the groundwater pool to the river	5.0×10^4	5.0×10^4
g	—	User defined exponent used to control the draining of the groundwater pool to the river	1.25	1.25

provided by the United Kingdom Met Office. Specifically, the HadCM3 coupled ocean-atmosphere global climate model[41–43] was used to provide lateral boundary conditions to drive the Met Office HadRM3P regional climate model.[44] While HadCM3 has a spatial resolution of 3.75° longitude by 2.5° latitude, the RCM (*i.e.* HadRM3P) has a much higher spatial resolution (0.22° × 0.22°, approximately 25 km), with 19 vertical levels and 4 soil levels. For this study the RCM covers a south Asia domain (with rotated pole coordinates of 260° longitude and 70° latitude), which allows for the development of full mesoscale circulations and captures important regional dynamics that occur remote from the specific areas of interest within the GBM catchments. Janes and Bhaskaran[40] have evaluated the HadRM3P simulations against a selection of high-resolution observational datasets, with a particular emphasis on the summer monsoon period of June to September. The RCM is found to be more skilful at reproducing both mean surface temperature patterns, and also performs better at simulating interannual variability in precipitation compared with the driving GCM. Given that sediment in the GBM catchments is dominantly transported during the monsoon months, and the importance of accurately simulating wet season precipitation when simulating these sediment loads, the use an RCM to force HydroTrend represents an important innovation of this study.

Simulations were run for the period 1971–2100 using observed greenhouse gas forcings for the historical period and the SRES A1B emissions scenario[45] for the future period. The SRES A1B scenario represents a medium-high emissions scenario that is consistent with much existing climate modelling work and which is fairly consistent with observed carbon emissions over the past two decades.[46,47] Furthermore, the HadCM3 simulations used to drive the RCM use a perturbed physics ensemble (PPE) approach, whereby key climate model parameters, which have an associated uncertainty, are perturbed within an ensemble of simulations to produce a range of projections which reflect the uncertainty in the parameters.[48–50]

In total, the Met Office has run 17 perturbed versions of HadCM3 with associated HadRM3P simulations for the 130 year period from 1971–2100.[40,51] However, to capture the range of these simulations and therefore their associated uncertainty, herein we employ only three members from this ensemble: referred to as the Q0, Q8 and Q16 runs, respectively (Table 2). The Q0 run was selected as the standard model run in that it exhibits a mid-range (of the full 17 member ensemble) climate sensitivity to the A1B emissions forcing. In contrast, Q16 has the highest climate sensitivity (*i.e.* it is the ensemble member that exhibits the highest global temperature response to the A1B emissions forcing) and was therefore selected to represent an extreme end member of the ensemble. In principle, Q1 represents the ensemble member with the lowest climate sensitivity, but this run was not used in this study. Instead, the Q8 run was selected because, although it has similar sensitivity to Q0, it exhibits a different precipitation response. Specifically, unlike the other ensemble members, the Q8 run shows a mid-century decrease in precipitation (Table 2). The inclusion of the Q8 run therefore enables the impacts on sediment transfer processes of this possible climate response to be accounted for, even if the likelihood of this response can be considered to be relatively low.

Although the RCM provides precipitation and temperature data at the daily time step resolution required by HydroTrend, as discussed in Section 2.1 HydroTrend is not a spatially explicit model. Consequently, the RCM data were post-processed for use in HydroTrend by spatially-averaging the RCM precipitation outputs (for each daily time step during the 1971–2100 simulation period) over the geographic extents of the two study catchments. The daily temperature data were taken from the RCM grid cells corresponding to the basin outlet points, as is required for input to HydroTrend (*i.e.* Farakka Barrage for the Ganges and the Jamuna–Ganges confluence for the Brahmaputra, see Fig. 1 for locations). The climate data sets used in the model simulations for each catchment are shown in Fig. 3.

3. Results and discussion

3.1. Assessment of model performance

Our assessment of HydroTrend initially focuses on evaluating the model's ability to estimate predictions of daily water discharge during the historical period, prior to comparing HydroTrend derived estimates of mean annual sediment flux (also in the historical period) to values cited in the literature. However, as discussed further below, one of the notable features of the Ganges and Brahmaputra river systems feeding the GBM delta complex is the lack of detailed empirical data on their sediment loads, rendering an assessment of HydroTrend's ability to estimate fluvial sediment delivery in these catchments challenging.

HydroTrend's ability to simulate water fluxes was assessed by comparing simulated and observed runoff regimes. An example of the model output (for flow discharge at daily resolution) is presented for the Ganges, for illustrative purposes, in Fig. 4. For

Table 2 Overview of the change in temperature and precipitation with respect to the annual mean for the 1981–2000 baseline period under the Q0, Q8 and Q16 Met Office RCM runs for the south Asia domain used in this study (for the SRES A1B emissions scenario)

	Mid century (2041–2060)		End of century (2080–2099)	
Climate model run	Temperature increase (K)	Precipitation increase (%)	Temperature increase (K)	Precipitation increase (%)
Q0	2.3	11.1	4.1	5.1
Q8	2.6	−9.9	4.1	12.7
Q16	2.6	12.2	4.6	29.5

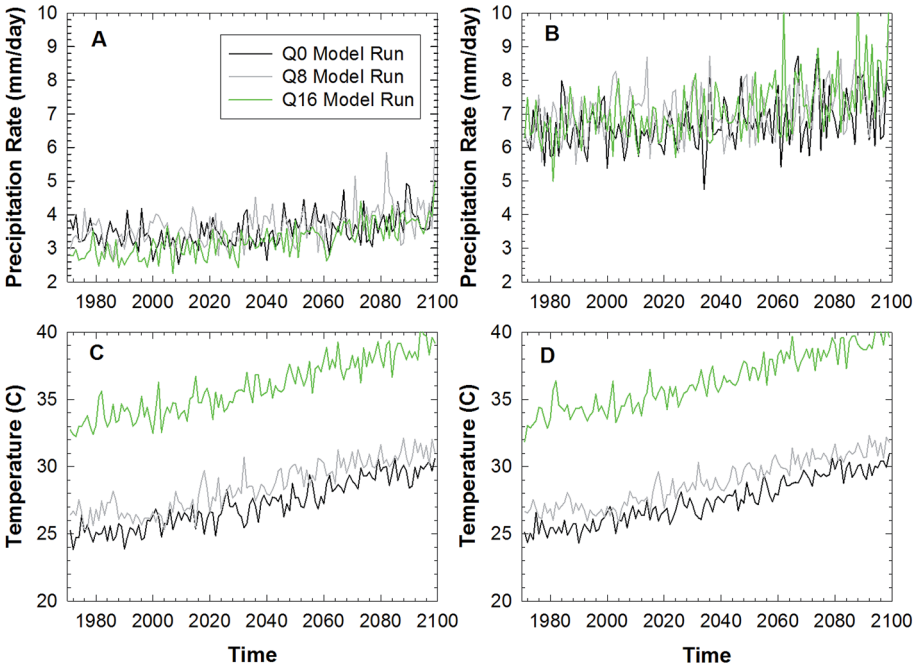

Fig. 3 Climate parameters used to force the HydroTrend simulations in this study for the period 1971–2100 and as obtained for three (Q0, Q8, Q16) perturbed ensemble runs of the HadRM3P Regional Climate Model (RCM) for a South Asia domain (see text for details of RCM set up and the model runs). The precipitation and temperature data time series used in HydroTrend simulations are at daily temporal resolution, but for clarity annual means are plotted here. Precipitation data are spatially-averaged over the geographic extent of each study catchment, whereas the temperature data are shown for each basin's outlet (see Fig. 1 for locations). The precipitation time series are shown for (a) the Ganges and (b) Brahmaputra basins, with the temperature time series shown in subplots (c) for the Ganges and (d) Brahmaputra.

clarity, the simulated water flux data presented in Fig. 4 are for the Q0 model run only. Furthermore, and again for reasons of clarity, the data in Fig. 4 are shown only for the period 1981–1990. We emphasise that the goodness of fit measures discussed below are derived for the entire period when the simulated data (which cover the period 1971–2100) overlap with flow years when there is no gap in the observed records. For both the Ganges and Brahmaputra this period of the overlapping record, used to assess HydroTrend's performance, is 1973 to 1995. In the analyses conducted below, it should also be noted that the model locations at which simulated data are obtained in each of the two study basins are not precisely spatially coincident with the closest available gauging stations (see Fig. 1). Specifically, for the Ganges simulations are undertaken at the Farakka Barrage, whereas observed flows are based on the gauging station located at Hardinge Bridge. For the Brahmaputra, simulations are undertaken at a location close to the confluence of the Jamuna with the Ganges, downstream of the gauging station at Bahadurabad.

Scatterplots of simulated *versus* observed daily discharges (for data from the Q0 model run) in the 1973–1995 assessment period are shown in Fig. 5a (for the Ganges) and Fig. 5b (for the Brahmaputra). It is evident that for both catchments there is a tendency for the model to over-predict higher flows, but to under-predict lower flows. The cross-over points, indicated where the red lines that represent the best fit between the simulated *versus* observed data intersect the black line indicating the 1 : 1 fit, are for both catchments close to the mean annual flows. Specifically, on the Ganges, the observed (at the Hardinge Bridge gauge) mean annual flow of 10 770 $m^3 s^{-1}$ is very close to the mean annual flow of 10 984 $m^3 s^{-1}$ simulated (at Farakka Barrage) under the Q0 model run, with the range of simulated mean annual flows varying between 9117 $m^3 s^{-1}$ (Q16 run) to 11 369 $m^3 s^{-1}$ (Q8 run). For the Brahmaputra, simulated mean annual flows fall within the range 20 492 $m^3 s^{-1}$ to 29 785 $m^3 s^{-1}$, depending on the climate model run, in comparison to the observed (at the Bahadurabad gauge) mean annual flow of 21 907 $m^3 s^{-1}$. As noted above, this latter observed value is close to the mean annual flow of 20 492 $m^3 s^{-1}$ simulated under the Q0 model run.

To further aid in evaluating the model's ability to simulate water fluxes emanating from each catchment, we supplement the information shown in the scatterplots (Fig. 5a for the Ganges and Fig. 5b for the Brahmaputra) with three other goodness-of-fit measures. First, to evaluate HydroTrend's ability to simulate flood flows we employ a mean discrepancy ratio (computed as the arithmetic mean of each ratio between the simulated and observed annual maxima in each year of the 1973–1995 record; $n = 22$). We regard HydroTrend's ability to simulate peak flows as being of particular significance for the current study since it is flood flows that contribute most to the transportation of fluvial sediment. Second, we derive the root mean square error (RMSE) of the simulated *versus* observed daily flows, and finally we compute the Nash–Sutcliffe Index[52] (NSI), again based on all daily flows in the 1973–1995 assessment period. These metrics are reported for each of the basins

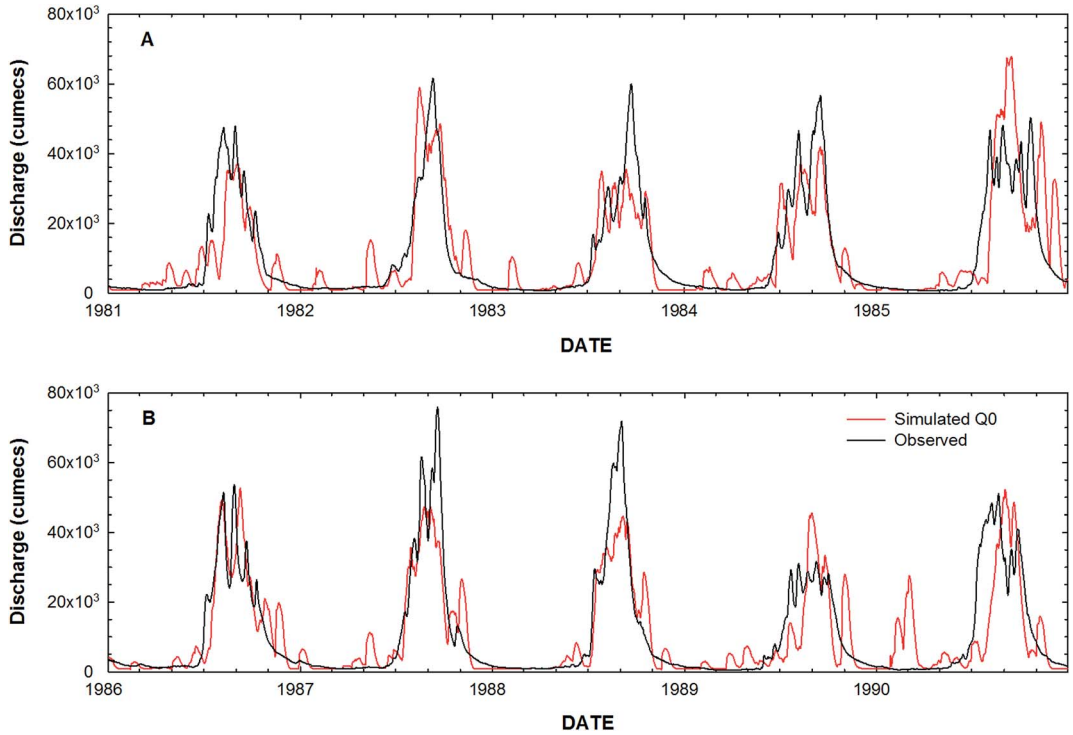

Fig. 4 Example of simulated daily discharges (at Farakka Barrage, for the Q0 climate model run only, which is the climate model run that gives the optimal fit to the observed data) for the Ganges for the periods (a) 1981–1985 and (b) 1986–1990. The daily flows observed at the Hardinge Bridge gauging station are also shown for comparison.

and for each climate change run in Table 3. These metrics confirm that HydroTrend, on average, tends to slightly under-predict annual maxima on the Ganges (Me = 0.950), but slightly over-predicts annual maxima on the Brahmaputra (Me = 1.113), with both these quoted values corresponding to the Q0 run. Furthermore, with a NSI value of 0.623, the overall model performance for the Ganges is considered to be "good" based on the classification scheme of Henriksen *et al.*,[53] but the 0.623 value falls very close to the threshold value (0.65) that would suggest a "very good" performance. For the Brahmaputra the NSI score of 0.420 is lower than for the Ganges. Consequently, HydroTrend's ability to simulate water fluxes in the Brahmaputra basin in classified as "poor" according to the Henriksen *et al.*[53] scheme, albeit with the 0.420 value of NSI being close to the threshold value of 0.50 required for the model to be considered "fair".

The simulated sediment loads for the baseline period (1981–2000) can be compared to estimates of sediment loads as derived from a range of empirical studies. However, when undertaking such comparisons it must be acknowledged that estimating sediment loads on large rivers is challenging. In particular, on both the Ganges and Brahmaputra studies of sediment loads have been sporadic and often of short duration, meaning that any individual estimate is subject to a high degree of uncertainty. For these reasons, we compare HydroTrend simulations of sediment load to empirical estimates of sediment load as obtained by a range of different authors. For example, Fig. 5c shows that empirical estimates of the sediment load on the Ganges range between 390 Mt per year[54] and 548 Mt per year (Delft Hydraulics and Danish Hydraulics Institute 1996, cited in Lupker *et al.*[54]). This range is also broadly consistent with the range, cited by both Milliman and Syvitski[55] and Wasson[56] of 440 to 520 Mt per year, and encompasses estimates derived from the suspended sediment rating curve of Islam *et al.*[21] for the Ganges at Hardinge Bridge. Specifically, when the Islam *et al.*[21] rating is applied using observed flow discharge values for the period 1981–1995 (the only years during the 1981–2000 baseline simulation period when a complete observed flow record is available), an estimated mean annual sediment load of 441 Mt per year is obtained. As indicated on Fig. 5c, this range of empirical estimates comfortably encompasses the mean annual sediment load simulated by HydroTrend for the 1981–2000 baseline period, with model estimates ranging between 475 Mt per year and 523 Mt per year, depending on the specific climate run used to force the model simulations.

For the Brahmaputra, Milliman and Syvitski[55] suggest the mean annual load is 540 Mt per year, a value that is substantiated by a better constrained estimate of 590 Mt per year derived from the Flood Action Plan[57] (discussed in Best *et al.*[58]). However, the suspended sediment rating curves developed by Islam *et al.*[21] for the Brahmaputra at Bahadurabad give a much higher estimate of 1109 Mt per year, when applied using observed flow data for the period 1981–1995 (as noted above, these are the only years with complete flow data during the 1981–2000 baseline period). Fig. 5d shows that the range of model simulated sediment loads (595 Mt per year to 672 Mt per year, depending on the specific climate model run) is slightly

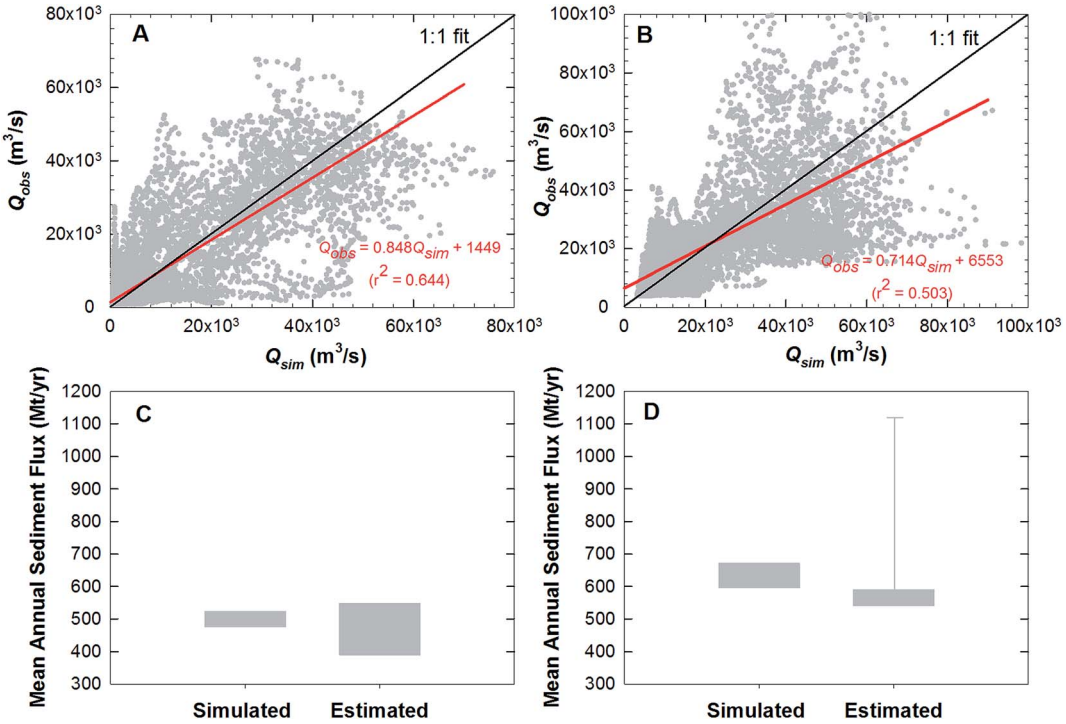

Fig. 5 Assessment of model performance in terms of daily flow discharges and mean annual sediment fluxes. Subplots (a) and (b) are scatterplots of simulated (Q_{sim}; for the Q0 climate model run) and observed (Q_{obs}) daily flow discharges during the period 1973–1995 for (a) the Ganges and (b) Brahamaputra Rivers (see Fig. 1 for model nodes in relation to the gauging stations used for the observed flow discharge data), with the line of best fit (red line) and its regression equation also shown. Subplots (c) and (d) are box plots indicating the range of estimates for mean annual sediment flux obtained firstly (labelled 'simulated') from the HydroTrend model (the spread of data indicating the range of data obtained across the Q0, Q8 and Q16 climate model runs) during the baseline (1981–2000) simulation period, but secondly (labelled 'estimated') the spread of estimates of sediment flux from a range of empirical studies for (c) the Ganges and (d) Brahmaputra Rivers (see text for details). The whisker shown in subplot (d) represents the sediment load estimated from the rating curve of Islam *et al.*[21] with observed flow data during 1981–1995 (see text for details).

Table 3 Overview of goodness of fit measures for simulated (for each of the three climate change runs explored in this study) *versus* observed water fluxes for the two study basins

	Climate change model run		
	Q0	Q8	Q16
Ganges basin			
Mean discrepancy ratio (annual peaks)	0.950	1.033	1.017
RMSE (m^3 s^{-1})	10 213	11 245	11 626
Nash–Sutcliffe Index	0.623	0.551	0.480
Brahmaputra basin			
Mean discrepancy ratio (annual peaks)	1.113	1.231	1.353
RMSE (m^3 s^{-1})	17 850	18 220	23 647
Nash–Sutcliffe Index	0.420	0.406	0.033

higher than the empirical estimates of Milliman and Syvitski[55] and Best *et al.*,[58] but it is within the range implied by the Islam *et al.*[21] rating curve, albeit with the latter plotted as an outlier on Fig. 5d.

The preceding brief synthesis of prior studies of sediment loads in the study region supports the notion that the Brahmaputra's load is higher than the Ganges, and that the long term combined total sediment flux from both basins is roughly in the range 1000 to 1100 Mt per year. The results of the HydroTrend simulations for the 1981–2000 baseline period are consistent with this, with the aggregated simulated loads from both catchments varying in the range 1116 Mt per year to 1147 Mt per year, across the three climate model runs. Likewise, the simulated proportion of the aggregated total that is derived from the Brahmaputra varies in the range 53–59%, depending on the specific climate model run. This consistency between our

model estimates of sediment flux in the baseline simulation period and the range of estimates cited by previous authors is encouraging, and for this reason we deem HydroTrend to be sufficiently reliable for the purposes of this study.

3.2. Impact of climate change on water and sediment flux

Annual water and sediment flux time series as simulated by HydroTrend for each climate change run were initially obtained for each individual year in the 1971–2100 simulation period by summing the daily model outputs. Mean annual water and sediment fluxes were then estimated by averaging over twenty year time-slices selected to represent current (baseline) conditions (1981–2000), conditions in the middle part of the 21st century (2041–2060), and conditions at the end of the 21st century (2080–2099), respectively (Fig. 6).

Fig. 6a shows that under the Q0 run mean annual flows for the Ganges are projected to increase relative to the 1981–2000 baseline of 10 984 $m^3 s^{-1}$, to 14 237 $m^3 s^{-1}$ by the 2050s and then 16 916 $m^3 s^{-1}$ by the end of the century, the latter representing an overall increase of 54% relative to the baseline period. Under the Q8 run mean annual flow reaches 17 549 $m^3 s^{-1}$ by the 2090s, which is an identical proportional increase of 54% with respect to the baseline period. For the Ganges, mean annual flows simulated for the Q16 run are less than both the Q0 and Q8 runs, reflecting the lower precipitation in this catchment for the Q16 run (see Fig. 3), but the proportional increase with respect to the baseline period is greater. Thus, for the Q16 run mean annual flow of 9117 $m^3 s^{-1}$ is simulated during the 1981–2000 baseline period, rising to 12 856 $m^3 s^{-1}$ by the 2050s (a 41% increase) and 16 136 $m^3 s^{-1}$ by the end of the century, an increase of 77% over the 1981–2000 Q16 baseline. Fig. 6b shows that, although simulated mean annual flows on the Brahmaputra are greater than for the Ganges, the proportional increases in flow simulated under future climate change are less. For example, mean annual flows are projected to rise from between 20 492 $m^3 s^{-1}$ and 29 785 $m^3 s^{-1}$ (depending on the climate model run) in the 1981–2000 baseline period to between 28 436 $m^3 s^{-1}$ and 36 679 $m^3 s^{-1}$ by the 2090s, an increase of between 23% and 39% relative to the baseline period, depending on the specific climate model run.

In terms of future sediment fluxes, Fig. 6c shows that under the Q0 run sediment loads on the Ganges are projected to significantly increase relative to the 1981–2000 baseline of 521 Mt per year, to 613 Mt per year by the 2050s and then 696 Mt per year by the end of the century, the latter representing an overall increase of 175 Mt per year (34%) relative to the baseline period. Under the Q8 run a similar increase in sediment load with time is also evident, with projected values of 609 Mt per year by the 2050s (a 16% increase relative to the Q8 baseline) and 714 Mt per year by the 2090s, an end of century value which

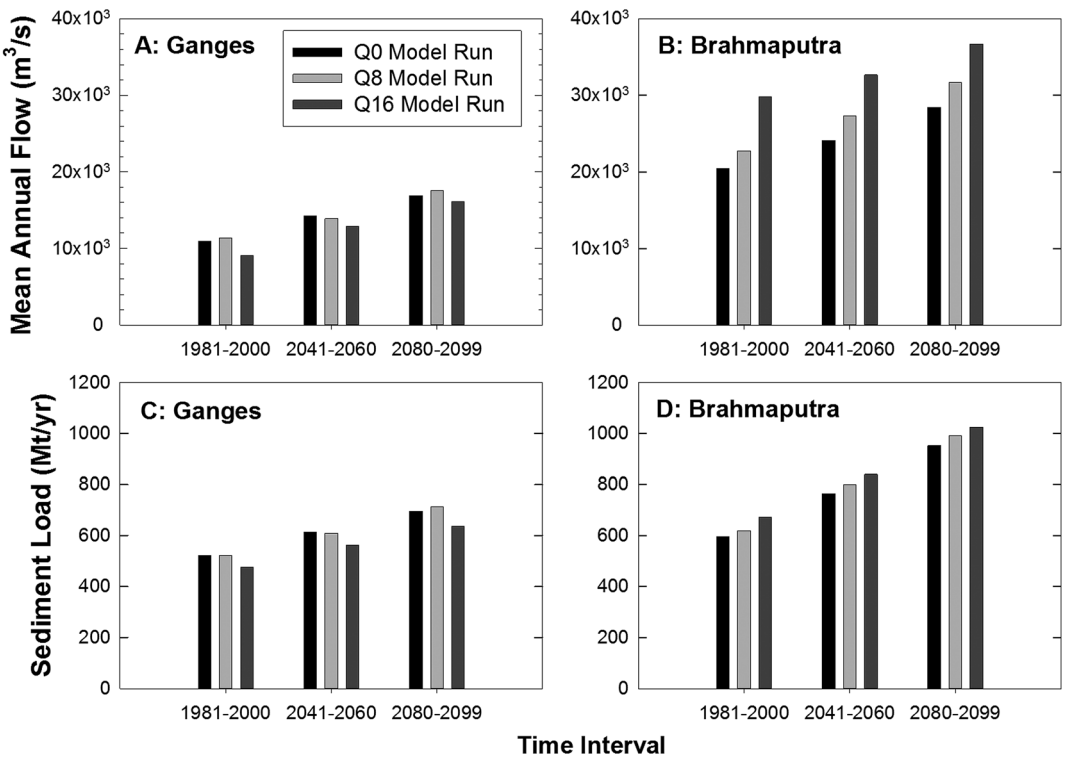

Fig. 6 Water and sediment fluxes as simulated by HydroTrend for a baseline (1981–2000) and two future (2041–2060 and 2080–2099) 20 year periods for the Ganges and Brahmaputra basins, with HydroTrend forced using climate data (shown in Fig. 3) for a range of climate model runs (Q0, Q8 and Q16) under the SRES A1B emissions scenario. Subplots (a) and (b) show mean annual flow discharges for the Ganges and Brahmaputra basins, respectively, while subplots (c) and (d) show mean annual sediment fluxes for the Ganges and Brahmaputra basins, respectively. Note that subplots (a) and (b), and subplots (c) and (d), are scaled identically to facilitate comparisons between model outputs for the Ganges and Brahmaputra catchments.

is around 191 Mt per year (37%) greater than the baseline. For the Ganges, sediment loads for the Q16 run are less than both the Q0 and Q8 runs, reflecting the lower precipitation in this catchment for the Q16 run (see Fig. 3). Thus, a mean annual sediment load of 475 Mt per year is simulated in the Q16 run during the 1981–2000 baseline period, rising to 562 Mt per year by the 2050s (an 18% increase) and 636 Mt per year by the end of the century, representing an increased load of 161 Mt per year (34%) over the 1981–2000 Q16 baseline.

For the Brahmaputra basin, there is a strong increase in sediment loads throughout the coming century under the anthropogenic climate change scenario (SRES A1B) investigated herein (Fig. 6d). For the Q0 run, sediment loads are projected to rise from 595 Mt per year in the 1981–2000 period through to 764 Mt per year by the 2050s (an increase of 28%) and then rise again to 952 Mt per year by the 2090s, an increase of some 357 Mt per year (60%) *versus* the baseline period. In the Q8 run, similar increases in sediment loads are projected, rising from 619 Mt per year in the baseline period through to 799 Mt per year (an increase of 29%) in the 2050s and 992 Mt per year by the 2090s, an end of century value that is 373 Mt per year (60%) greater than in 1981–2000. In the Q16 run the simulated sediment loads in the 1981–2000 baseline period are considerably larger than in the other runs and rise to 839 Mt per year and 1024 Mt per year by the 2050s and 2090s, respectively, the latter being an overall increase of 352 Mt per year. This change represents a slightly smaller proportional increase relative to the baseline (25% and 52%, respectively) over the Q0 and Q8 runs.

Prior to discussing any inter-basin differences in the simulated response of fluvial sediment loads to future climate change and the significance of these simulated future changes, it should be noted that for both catchments there are uncertainties associated with the predicted values of future sediment fluxes that arise as a consequence of the range in the perturbed HadRM3P RCM-derived climatologies used to drive the HydroTrend simulations. However, these uncertainties are quite small: the overall ranges (across the Q0, Q8 and Q16 model runs) of predicted end of century (2090s) sediment loads are 78 Mt per year and 72 Mt per year for the Ganges and Brahmaputra, respectively; ranges that are within only ±11% (Ganges) and ±8% (Brahmaputra) of the 'standard' Q0 run totals. Moreover, for the Ganges the predicted increases in future sediment flux are sufficiently large that, by the 2050s, they exceed the uncertainties in the contemporary estimates of sediment flux (see Fig. 5c and d). That is for the Ganges, by the 2050s, the increased fluvial sediment flux 'signal' exceeds the uncertainties associated with using the RCM climatologies. The results are less clear for the Brahmaputra, but they are replicated if the single outlying estimate of contemporary sediment flux (see Fig. 5d) attributed to the rating curve of Islam *et al.*[21] is discarded. If that latter estimate is retained, a clear increase in future sediment flux *versus* contemporary estimates on the Brahmaputra eventually emerges by the 2090s. Within this context it can also be noted that the end of century (2090s) predicted increases in future sediment flux from the Brahmaputra (of between 52% and 60%) are proportionally greater than the predicted increases in sediment flux from the Ganges (of between 34% and 37%), even though the simulated increases in water flow discharges are smaller for the former than the latter. The greater sensitivity, relative to the Ganges, of the Brahmaputra's fluvial sediment loads to the climate change scenario investigated herein, is readily explained by the important influence of increasing temperatures (see Fig. 3 and eqn (4)) in the Brahmaputra basin, which has a much greater proportion of its terrain at higher elevations (see Fig. 1 and 2). Consequently, rising temperatures in the more heavily glaciated Brahmaputra basin have a stronger impact on sediment loads than in the less elevated Ganges basin.

It is evident from the above that substantial increases in sediment loads are predicted to occur under the climate change scenario explored in this study. Specifically, the increases in end of century sediment loads that are projected from the Ganges (which range from an additional 161 Mt per year under the Q16 run to 191 Mt per year for Q8) and Brahmaputra (352 Mt per year under the Q16 run to 373 Mt per year under the Q8 run) amount to a combined increase of between 513 Mt per year and 564 Mt per year emanating from the two river systems. This represents an increase of around 50% over and above contemporary sediment loads. This raises an intriguing and important question: are these increases sufficient to buffer, through accelerated sedimentation, the adverse impacts of climate-change driven sea level rise in the GBM delta? Initially making the very crude assumption that *all* this additional sediment from the Ganges

Table 4 Delta sedimentation rates may increase in response to the increases in fluvial sediment loads predicted in this study. The range of likely future sedimentation rate may be constrained by our upper bound estimate of end of century sedimentation rates (see text for details) and mean contemporary aggradation rates in different parts of the delta, the latter as synthesised from Wilson and Goodbred[25]

		Fluvial-tidal delta	
Description	Fan delta	Interior (fluvial backwater)	River mouth (tidal)
Upper bound limit of end of century aggradation rate (mm per year) (this study)	48–53		
Contemporary sedimentation rates in regions of delta that are being *constructed*[25]	10 ± 5	10 ± 5	15 ± 5
Contemporary sedimentation rates in regions of delta that are being *maintained*[25]	0 ± 3	−3 ± 3	10 ± 5

and Brahmaputra (*i.e.* 513 to 564 Mt per year) were retained on the surface of the eastern delta (which covers an area of ~10 000 km^2), and further assuming an unconsolidated bulk density of ~1060 kg m^{-3}, suggests that spatially-averaged deposition rates in the eastern part of the delta could be ~48 to 53 mm per year greater than they are now by the end of the century. It is important to recognise that this estimate represents an absolute upper bound on what is possible: in reality, not all this additional sediment would be retained on the surface of the delta and deposition is not distributed uniformly across the delta complex (*e.g.* see Fig. 2b of Wilson and Goodbred[25]). A recent synthesis[25] of contemporary sedimentation within different components of the delta complex offers a sensible lower bound estimate for future sedimentation rates. We therefore speculate that the increased sediment loads projected in our study may result in sedimentation rates that fall between these limits (Table 4).

Since any additional accretion is cumulative, such increases in sediment loads could provide a substantial degree of additional resilience to the accelerated sea-level rise, of up to 1 m or more, that is projected to occur, due to climate change and/or increased subsidence, in the forthcoming century.[11] However, an important limitation on our results is that only climate change has been considered. Other catchment changes, such as increased water transfers and catchment storage,[59] may occur. Within the delta, flood defences and polders also exclude sedimentation except in extreme floods.[60] Using controlled sedimentation in polders to build elevation as sea levels rise is now recognised as a possible, but untested response in Bangladesh,[61] as well as in other vulnerable deltas across the globe. Hence, further research on all these issues is urgently required, including refining and improving estimates of present and future sediment fluxes to the GBM delta.

4. Conclusion

This study offers the first estimate of how anthropogenic climate change will affect the delivery of fluvial sediment to the Ganges–Brahmaputra–Meghna (GBM) delta over the course of this century. A climate-driven hydrological water balance and transport model (HydroTrend) was employed to simulate water discharge and sediment load at the points at which the Ganges and Brahmaputra flow into the GBM delta complex. HydroTrend was parameterised using high-quality topographic data and forced, for the period 1971–2100, using temperature and precipitation data from downscaled Regional Climate Model simulations using variants of the SRES A1B emissions scenario. A comparison of simulated and observed water and sediment fluxes during the historical period was undertaken to confirm HydroTrend's suitability for use in this study.

The key finding of this study is that fluvial sediment delivery to the GBM delta is projected to increase under the influence of anthropogenic climate change, albeit with the magnitude of the increase varying according to the specific catchment being considered. By the middle part of the 21st century, we find that sediment loads are projected to increase by between 16% and 18% for the Ganges, and between 25% and 30% for the Brahmaputra. As noted previously, a mid-century decrease in precipitation is simulated for the Q8 model run (see Table 2), but mid-century sediment loads under the Q8 run nevertheless increase on the Ganges and Brahmaputra, due to rising snow melt dominating over the reduced precipitation. We also find that, as precipitation increases towards the end of the 21st century, the projected increase in sediment flux emanating from the two catchments increases further, reaching between 34% and 37% for the Ganges, and between 52% and 60% for the Brahmaputra, by the 2090s, respectively. It is important to note that for both catchments the uncertainty, associated with the future sediment fluxes predicted for the 2050s and 2090s across the perturbed HadRM3P RCM-derived SRES climatologies is relatively small. Moreover, for the Ganges the simulated increases in predicted sediment fluxes are sufficiently large that, by the 2050s, they exceed the uncertainties associated with contemporary estimates of sediment flux (see Fig. 5c and d). In other words, the increased fluvial sediment flux 'signal' exceeds the uncertainties associated with the RCM climatologies by the 2050s. This is less clear for the Brahmaputra due to the outlier estimate based on the rating curve of Islam *et al.*[21] However, even if that latter estimate is retained, then a clear increase in future sediment flux *versus* contemporary estimates still emerges for the Brahmaputra by the 2090s.

These findings are significant for assessments of the future sustainability and resilience of the GBM delta which is one of the world's most vulnerable mega-deltas. An increase in climate-driven fluvial sediment flux has the potential, through accelerated aggradation on the delta surface, to buffer some of the deleterious impacts of climate change that are associated with rising sea levels in the Bay of Bengal and which threaten the vulnerable GBM delta. The projected increase in sediment flux emanating from the GBM delta's sub-continental scale catchments therefore represents a potentially beneficial impact of climate change (for the delta and its inhabitants). However, these potential beneficial impacts of climate change remain subject to uncertainty and can only be expressed if more sediment actually reaches the delta. This may not be the case if anthropogenic disturbances within the feeder catchments, notably due to existing and proposed future construction of major dams, result in the delta becoming increasingly disconnected from the sediment supply that sustains it. Disconnection also occurs within the delta due to flood defences and polders, although interest in controlling sedimentation is growing. These aspects are important topics for further research.

Acknowledgements

This research is part of the ESPA Deltas consortium (https://www.espadelta.net), a project of the NERC/ESRC/DfiD Ecosystem Services and Poverty Alleviation Thematic Programme funded by award NE/J002755/1. The ASTER L1B data product was obtained through the online Data Pool at the NASA Land Processes Distributed Active Archive Center (LP DAAC), USGS/Earth Resources Observation and Science (EROS) Center, Sioux Falls, South Dakota (https://lpdaac.usgs.gov/data_access). We thank John Ceasar (UK Met Office) for providing the climate

data sets used herein. Finally, we thank Irina Overeem and one anonymous reviewer for their highly constructive reviews of the first version of this paper.

References

1 S. Cohen, A. J. Kettner and J. P. M. Syvitski, *Global Planet. Change*, 2014, **115**, 44–58.
2 J. D. Pelletier, *J. Geophys. Res.: Atmos.*, 2012, **117**, DOI: 10.1029/2011F002129.
3 C. J. Vörösmarty, K. P. Sharma, B. M. Fekete, A. H. Copeland, J. Holden, J. Marble and J. A. Lough, *Ambio*, 1997, **26**, 210–219.
4 J. P. M. Syvitski and J. D. Milliman, *J. Geol.*, 2007, **115**, 1–19.
5 J. P. Ericson, C. J. Vörösmarty, S. L. Dingman, L. G. Ward and M. Meybeck, *Global Planet. Change*, 2006, **50**, 63–82.
6 J. P. M. Syvitski, A. J. Kettner, I. Overeem, E. W. H. Hutton, M. T. Hannon, G. R. Brakenridge, J. Day, C. Vörösmarty, Y. Saito, L. Giosan and R. J. Nicholls, *Nat. Geosci.*, 2009, **2**, 681–686.
7 P. Nutalaya, R. N. Yong, T. Chumnankit and S. Buapeng, in *Sea-Level Rise and Coastal Subsidence: Causes, Consequences, and Strategies*, ed. J. D. Milliman and B. U. Haq, Springer Science & Business Media, Dordrecht, 1996, pp. 105–130.
8 S. A. Higgins, I. Overeem, M. S. Steckler, J. P. M. Syvitski, L. Seeber and S. H. Akhter, *J. Geophys. Res.: Atmos.*, 2014, **119**, 1768–1781.
9 S. Brown and R. J. Nicholls, *Sci. Total Environ.*, 2015, **527–528**, 362–374.
10 M. Rhein, *et al.*, in *Climate Change 2013: The Physical Science Basis. Contribution of Working Group I to the Fifth Assessment Report of the Intergovernmental Panel on Climate Change*, ed. T. F. Stocker, *et al.*, Cambridge University Press, Cambridge, 2013.
11 J. A. Church, *et al.*, in *Climate Change 2013: The Physical Science Basis. Contribution of Working Group I to the Fifth Assessment Report of the Intergovernmental Panel on Climate Change*, ed. T. F. Stocker, *et al.*, Cambridge University Press, Cambridge, 2013.
12 D. E. Walling, *Hydrobiologia*, 1999, **410**, 223–240.
13 D. E. Walling, *Geomorphology*, 2006, **79**, 192–216.
14 D. E. Walling and D. Fang, *Global Planet. Change*, 2003, **39**, 111–126.
15 J. P. M. Syvitski, *J. Sustainability Sci. Manage.*, 2007, **3**, 23–32.
16 H. Gupta, S. Kao and M. Dai, *J. Hydrol.*, 2012, **464–465**, 447–458.
17 J. W. Day, D. F. Boesch, E. J. Clairain, G. P. Kemp, S. B. Laska, W. J. Mitsch, K. Orth, H. Mashriqui, D. J. Reed, L. Shabman, C. A. Simenstad, B. J. Streever, R. R. Twilley, C. C. Watson, J. T. Wells and D. F. Whigham, *Science*, 2007, **315**, 1679–1684.
18 J. A. Nittrouer, J. L. Best, C. Brantley, R. W. Cash, M. Czapiga, P. Kumar and G. Parker, *Nat. Geosci.*, 2012, **5**, 534–537.
19 A. J. Kettner and J. P. M. Syvitski, *Comput. Geosci.*, 2008, **34**, 1170–1183.
20 S. Cohen, A. J. Kettner, J. P. M. Syvitski and B. M. Fekete, *Comput. Geosci.*, 2013, **53**, 80–93.
21 M. R. Islam, S. F. Begum, Y. Yamaguchi and K. Ogawa, *Hydrol. Processes*, 1999, **13**, 2907–2923.
22 M. H. Sarker and C. R. Thorne, in *Braided Rivers: Process, Deposits, Ecology and Management*, ed. G. H. Sambrook Smith, J. L. Best, C. S. Bristow and G. E. Petts, Blackwell Publishing Ltd, Oxford, 2006.
23 C. D. Woodroffe, R. J. Nicholls, Y. Saito, Z. Chen and S. L. Goodbred, in *Global change and integrated coastal management*, ed. N. Harvey, Springer, The Netherlands, 2006, pp. 277–314.
24 S. L. Goodbred and S. A. Kuehl, *Geology*, 1999, **27**, 559–562.
25 C. A. Wilson and S. L. Goodbred, *Annual Review of Marine Science*, 2015, **7**, 67–88.
26 A. J. Kettner and J. P. M. Syvitski, in *Analogue and Numerical Modelling of Sedimentary Systems: From Understanding to Prediction*, ed. P. de Boer, G. Postma, K. van der Zwan, P. Burgess and P. Kukla, Wiley-Blackwell, Oxford, UK, 2008, ch. 7, DOI: 10.1002/9781444303131.
27 B. Gomez, Y. Cui, A. J. Kettner, D. H. Peacock and J. P. M. Syvitski, *Global Planet. Change*, 2009, **67**, 153–166.
28 P. Upton, A. J. Kettner, B. Gomez, A. R. Orpin, N. Litchfield and M. J. Page, *Comput. Geosci.*, 2013, **53**, 48–57.
29 J. P. M. Syvitski and A. J. Kettner, *Cont. Shelf Res.*, 2007, **27**, 296–308.
30 J. P. M. Syvitski and J. M. Alcott, *Comput. Geosci.*, 1995, **27**, 731–753.
31 J. P. M. Syvitski, S. D. Peckham, R. Hilberman and T. Mulder, *Sediment. Geol.*, 2003, **162**, 4–24.
32 C. B. Brown, *Trans. Am. Soc. Civ. Eng.*, 1944, **109**, 1047–1106.
33 G. M. Brune, *Trans., Am. Geophys. Union*, 1953, **34**, 407–418.
34 C. J. Vörösmarty, M. Meybeck, B. Fekete, K. Sharma, P. Green and J. P. M. Syvitski, *Global Planet. Change*, 2003, **39**, 169–190.
35 NASA Land Processes Distributed Active Archive Center (LP DAAC), *2ASTER L1B.USGS/Earth Resources Observation and Science (EROS) Center*, South Dakota, Sioux Falls, USA, 2001.
36 S. Ya-feng, H. Tze-chu, C. Pen-hsing, and L. Chi-chun, *World Glacier Inventory: Proceedings of the Riederalp Workshop*, 1980, vol. 126, pp. 111–116.
37 B. Lehner, C. R. Liermann, C. Revenga, C. Vörösmarty, B. Fekete, P. Crouzet, P. Döll, M. Endejan, K. Frenken, J. Magome, C. Nilsson, J. C. Robertson, R. Rödel, N. Sindorf and D. Wisser, *Front. Ecol. Environ.*, 2011, **9**, 494–502.
38 B. Lehner, C. R. Liermann, C. Revenga, C. Vörösmarty, B. Fekete, P. Crouzet, P. Döll, M. Endejan, K. Frenken, J. Magome, C. Nilsson, J. C. Robertson, R. Rödel, N. Sindorf and D. Wisser, *Global Reservoir and Dam Database, Version 1 (GRanDv1)*, NASA Socioeconomic Data and Applications Center (SEDAC), Palisades, NY, 2001, http://sedac.ciesin.columbia.edu/data/collection/grand-v1, accessed 06/08/2014.
39 N. J. Clifford, in *The History of the Study of Landforms*, ed. T. P. Burt, R. J. Chorley, D. Brunsden, N J. Cox and A. S. Goudie, Geological Society of London, London, 2008.

40 T. Janes and B. Bhaskaran, *Evaluation of regional model performance in simulating key climate variables over Bangladesh*, Met Office, United Kingdom, 2012.
41 C. Gordon, C. Cooper, C. A. Senior, H. Banks, J. M. Gregory, T. C. Johns, J. F. B. Mitchell and R. A. Wood, *Clim. Dynam.*, 2000, **16**, 147–168.
42 V. D. Pope, M. L. Gallani, P. R. Rowntree and R. A. Stratton, *Clim. Dynam.*, 2000, **16**, 123–146.
43 M. Collins, S. F. B. Tett and C. Cooper, *Clim. Dynam.*, 2001, **17**, 61–81.
44 R. G. Jones, M. Noguer, D. C. Hassell, D. Hudson, S. S. Wilson, G. J. Jenkins and J. F. B. Mitchell, *Generating high resolution climate change scenarios using PRECIS*, Met Office Hadley Centre, Exeter, UK, 2004, p. 40, http://www.metoffice.gov.uk/precis/support.
45 N. Nakicenovic and R. Swart, *Special Report on Emissions Scenarios: A Special Report of Working Group III of the Intergovernmental Panel on Climate Change*, Cambridge University Press, Cambridge, UK, 2000, p. 599.
46 D. van Vuuren and K. Riahi, *Clim. Change*, 2008, **91**, 237–248.
47 C. le Quéré, *Nat. Geosci.*, 2009, **2**, 831–836.
48 J. M. Murphy, D. M. H. Sexton, D. M. Barnett, G. S. Jones, M. J. Webb, M. Collins and D. A. Stainforth, *Nature*, 2004, **430**, 768–772.
49 M. Collins, B. B. B. Booth, G. R. Harris, J. M. Murphy, D. M. H. Sexton and M. J. Webb, *Clim. Dynam.*, 2006, **27**, 127–147.
50 M. Collins, B. B. B. Booth, B. Bhaskaran, G. R. Harris, J. M. Murphy, D. M. H. Sexton and M. J. Webb, *Clim. Dynam.*, 2010, **36**, 1737–1766.
51 J. Caesar, T. Janes, A. Lindsay and B. Bhaskaran, *Environ. Sci.: Processes Impacts*, 2015, **17**, 1047–1056.
52 J. E. Nash and J. V. Sutcliffe, *J. Hydrol.*, 1970, **10**, 282–290.
53 H. J. Henriksen, L. Troldborg, A. J. Hojberg and J. C. Refsgaard, *J. Hydrol.*, 2008, **348**, 224–240.
54 M. Lupker, C. France-Lanord, J. Lavé, J. Bouchez, V. Galy, F. Métivier, J. Gaillardet, B. Lartiges and J.-L. Mugnier, *J. Geophys. Res.: Earth Surf.*, 2011, **116**, DOI: 10.1029/2010JF001947.
55 J. D. Milliman and J. P. M. Syvitski, *J. Geol.*, 1992, **100**, 525–544.
56 R. J. Wasson, *Curr. Sci.*, 2003, **84**, 1041–1047.
57 FAP 24, *River Survey Project (Main Report), Water Resources, Planning Organization*, Bangladesh, 1996.
58 J. L. Best, P. J. Ashworth, M. Sarker and J. E. Roden, in *Large Rivers: Geomorphology and Management*, ed. A. Gupta, Wiley, Chichester, 2001.
59 P. G. Whitehead, S. Sarkar, J. Lin, M. N. Futter, J. Caesar, E. Barbour, D. Butterfield, R. Sinha, R. J. Nicholls, C. W. Hutton and H. D. Leckie, *Environ. Sci.: Processes Impacts*, 2015, **17**, 1082–1097.
60 L. W. Auerbach, S. L. Goodbred, D. R. Mondal, C. A. Wilson, K. R. Ahmed, K. Roy, M. S. Steckler, C. Small, J. M. Gilligan and B. A. Ackerly, *Nat. Clim. Change*, 2015, **5**, 153–157.
61 H. Brammer, *Climate Risk Management*, 2014, **1**, 51–62.